

Tunneling emission from self-organized In(Ga)As/GaAs quantum dots observed via time-resolved capacitance measurements

M. Geller,* E. Stock, C. Kapteyn, R. L. Sellin,[†] and D. Bimberg

Institut für Festkörperphysik, Technische Universität Berlin, Hardenbergstraße 36, 10623 Berlin, Germany

(Received 20 June 2005; revised manuscript received 13 January 2006; published 17 May 2006)

The observation of tunneling emission of electrons and holes from In(Ga)As/GaAs quantum dots in time-resolved capacitance measurements is reported. The electron and hole ground-state localization energies are determined as (290 ± 30) meV and (210 ± 20) meV, respectively. These energies are in excellent agreement with predictions from eight-band $\mathbf{k} \cdot \mathbf{p}$ theory. Based on the localization energies, we estimate the escape time for thermal excitation at room temperature as ~ 200 ns for electrons and ~ 0.5 ns for holes in case of a zero-electric-field situation. The electric-field dependence of the tunneling emission is investigated in detail.

DOI: [10.1103/PhysRevB.73.205331](https://doi.org/10.1103/PhysRevB.73.205331)

PACS number(s): 73.21.La, 73.63.Kv

I. INTRODUCTION

Self-organized semiconductor quantum dots (QDs) (Ref. 1) with their peculiar electronic and optical properties resembling artificial atoms can be regarded as building blocks for various optoelectronic devices such as semiconductor lasers,^{2–4} ultrahigh-frequency applications,⁵ single-photon sources,^{6,7} and detectors.^{8,9} QD-based lasers are the most obvious and widely investigated application. However, self-organized QDs are also very interesting as an alternative approach for future single-electron memories.^{10–14} The understanding of the carrier escape mechanisms from QDs is a crucial prerequisite for any application of self-organized QDs in electronics. Thermally activated and tunneling carrier emission are the essential processes, which limit the storage time of memory devices. The inherent QD property which determines the thermal and tunneling emission time constants is the ground-state localization energy of the electrons or holes.

In this paper, we report the observation of tunneling emission of electrons and holes from the ground states of In(Ga)As/GaAs QDs using time-resolved capacitance measurements. By this method, the tunneling times as function of an applied electric field can be derived. A time-dependent decrease of the electron or hole ground state population is observed which is due to pure tunneling escape at low temperatures, where thermally activated emission is negligible. In addition, by measuring the tunneling time as function of the electric-field strength, we are able to determine the electron and hole localization energy with high accuracy. This time-resolved tunneling capacitance measurement (TRTCM) allows one to determine localization energies that are in excellent agreement with calculations based on eight-band $\mathbf{k} \cdot \mathbf{p}$ theory.¹⁵ The thermally activated escape times at room temperature are determined from the localization energies. These escape times finally limit the carrier storage time in device applications where no electric field is present and therefore tunneling is suppressed.

Space-charge transient methods^{16,17} as deep level transient spectroscopy (DLTS) has been used successfully to study thermal emission processes and thermal activation energies of QD systems.^{18–24} These thermal activation energies, however, do not represent the localization energies of the charge

carriers, as the underlying physical mechanism is a two-stage escape process: Thermal activation from the QD ground or an excited state into an intermediate state and subsequent tunneling through the remaining triangular barrier.^{21,24,25} The activation energy equals the separation energy between these two energy levels. Therefore, the correct QD localization energies cannot easily be observed in conventional DLTS measurements, due to this competing tunneling in an applied electric field. The TRTCM enables one to determine these important values for zero-dimensional In(Ga)As self-organized QDs with high accuracy.

II. SAMPLE STRUCTURE

Two samples were used to investigate the electron and hole tunneling emission from self-organized QDs. Both were grown using metalorganic chemical vapor deposition (MOCVD) on a GaAs(001) substrate. The QD layer was incorporated in either a p^+n - or a n^+p -diode structure to allow controlled charging of the electron and hole states, respectively. The QDs are outside the depletion region without bias and thus completely charged in the conductive surroundings. If the surrounding material is p -doped/ n -doped, the QDs are charged with holes/electrons, respectively. By increasing the reverse bias, the QDs can be successively depopulated of charge carriers and finally become neutral.

The first sample, referred to as H1—to study the hole tunneling—is a n^+p structure containing a single In_xGa_{1-x}As/GaAs QD layer formed by deposition of ~ 3 monolayers In_{0.8}Ga_{0.2}As at 500 °C. The QD sheet-density amounts to $N_D^{\text{H1}} \approx 3 \times 10^{10} \text{ cm}^{-2}$. The QDs exhibit a ground-state transition at ~ 1.12 eV as observed by photoluminescence at He temperature,²⁶ and an average QD base length of about 16 nm. On top of a GaAs(001) substrate, a 500 nm thick highly p -doped GaAs ($\sim 1 \times 10^{18} \text{ cm}^{-3}$) layer followed by 700 nm slightly p -doped ($\sim 3 \times 10^{16} \text{ cm}^{-3}$) GaAs were deposited. Subsequently, on top of a 10 nm thick undoped GaAs layer, ~ 3 ML In_{0.8}Ga_{0.2}As were deposited forming the self-organized QDs. The QDs were eventually overgrown with 7 nm undoped GaAs and a 500 nm layer of slightly p -doped ($\sim 3 \times 10^{16} \text{ cm}^{-3}$) GaAs. Finally, a 400 nm highly n -doped ($\sim 7 \times 10^{18} \text{ cm}^{-3}$) GaAs cap layer formed the n^+ contact.

The second sample, referred to as sample E1, is a p^+n structure with $\text{In}_x\text{Ga}_{1-x}\text{As}/\text{GaAs}$ QDs embedded in the n -doped region, to study electron tunneling. The $\text{In}_x\text{Ga}_{1-x}\text{As}$ QDs were grown at 500°C by deposition of ~ 7 ML $\text{In}_{0.7}\text{Ga}_{0.3}\text{As}$ on top of a QD seed layer, which was formed by the deposition of ~ 3.5 ML $\text{In}_{0.7}\text{Ga}_{0.3}\text{As}$ QDs. The GaAs spacer of only 3 nm thickness ensures vertical growth correlation between the two QD layers. The QDs of the second layer nucleate directly above the QDs of the seed layer, and also have a bigger size than the seed QDs. This method was used to achieve a high QD density of large $\text{In}_x\text{Ga}_{1-x}\text{As}$ QDs.²⁷ Transmission electron microscopy (TEM) images of comparable samples²⁸ show a QD area density of $\sim 5 \times 10^{10} \text{ cm}^{-2}$, a truncated pyramidal shape with an average base width of about 18–20 nm and a height of ~ 4 nm. The ground-state transition energy in PL is ~ 1.04 eV at He temperatures.²⁶ The smaller $\text{In}_x\text{Ga}_{1-x}\text{As}$ seed QDs have only a minor impact on the electronic and optical properties of the $\text{In}_x\text{Ga}_{1-x}\text{As}$ QDs due to the large mismatch of the ground-state transition energies of the two QD types.²⁹

For both samples, photolithography and chemical wet etching were employed to form mesa structures with a diameter of $800 \mu\text{m}$. Ohmic contacts were formed on top and back of the structures by metal evaporation and alloying. With a diameter of $800 \mu\text{m}$ of the mesa structure and an average QD sheet density of $3 \times 10^{10} \text{ cm}^{-2}$ we observe in the following experiments always the carrier emission from an energy broadened ensemble of millions of QDs. The energy broadening is due to fluctuations in size, shape, and composition of single QDs in the ensemble.

III. EXPERIMENTAL RESULTS

A. Static capacitance-voltage measurements

Figure 1 depicts the static capacitance-voltage (C - V) trace (solid line) of samples H1 (a) and E1 (b), recorded at $T = 100$ K at a modulation frequency of 1 kHz. In both C - V curves, a pronounced plateau is visible which reflects the charge accumulation in the QD layer. For sample H1, the depletion region of the n^+p diode reaches the QD layer at a reverse bias of about 7.0 V and is pinned there, precisely marked by a maximum of the second derivative (dashed line) in Fig. 1(a). As a consequence, the capacitance remains roughly constant for increasing reverse bias until all holes are removed from the QDs at 9.4 V. The small quantization energies of the hole levels do not allow to distinguish between the population of ground and excited states in the C - V measurement. For sample E1 in Fig. 1(b), the onset of the plateau at a reverse bias of about 6.5 V, as marked by the peaks of the second derivative (dashed line), denotes the beginning of the population of the electron ground states. The larger level splitting of the electron states here one allows to distinguish between ground and excited state population. Between 6.5 V and 5.5 V, the ground state is populated with two electrons. The excited states are populated with electrons below 5.5 V, whereas below 3.0 V the QDs leave the space-charge region and are completely filled.

The C - V results enable us to estimate the number of charge carriers accumulated in the QD layer from: Q

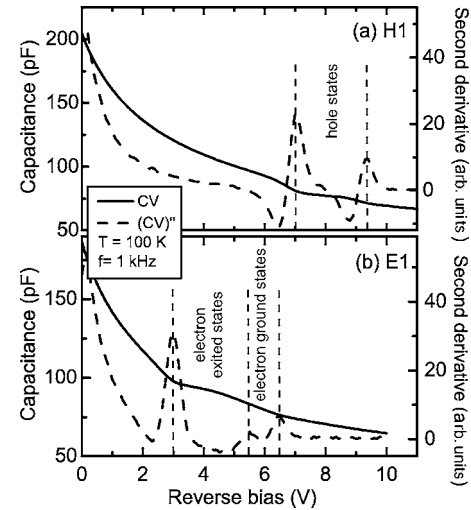


FIG. 1. Static C - V characteristics of sample (a) H1 and (b) E1 at $T = 100$ K for a measurement frequency of $f = 1$ kHz (solid line). The plateau in the C - V traces is due to hole or electron accumulation, respectively, in the QD layer. The maxima of the second derivative (dashed line) precisely indicate the beginning and end of the plateaus.

$\approx C_p \Delta V$, where C_p is the capacitance of the plateau region, and ΔV is the width of the plateau. In addition, knowledge of the QD area density is required to evaluate the average population of completely charged QDs. For sample H1, a maximum number of approximately seven holes per QD is found. For sample E1, the evaluation of the C - V data yields two charge carriers per QD for the reverse bias region from 5.5 V to 6.5 V, as expected for a spin-degenerated ground state. Five more electrons can be charged into the excited state for the voltage region between 3.0 V to 5.5 V. In total, sample E1 can be charged with up to seven electrons per QD.

The C - V characterization reveals the bias needed to charge the different QD levels in the following DLTS and TRTCM experiments. Precise bias values are required for the TRTCM method where only the electron/hole ground states will be populated with charge carriers.

B. Thermally activated charge carrier emission

In this section, we discuss the thermally activated emission from the QDs, as also previously observed in conventional DLTS measurements,^{20,21,23,24} in order to compare this results with the outcome from the TRTCM method.

Figure 2(a) depicts two DLTS measurements of sample H1 for a pulse bias of $V_p = 7.0$ V and 9.2 V. The reverse bias was fixed to $V_r = 9.4$ V. For a reverse bias of 9.4 V, the QDs are inside the depletion region, i.e., they are totally depleted from charge carriers [cf. the C - V measurement in Fig. 1(a)]. At a pulse bias of $V_p = 7.0$ V, the QDs are completely filled with holes during a 10 ms electrical pulse. After the bias is set back to the starting situation, the QDs are again in the depletion region in a nonequilibrium state with the reservoir and all trapped holes are emitted (see schematic picture in [Fig. 2(a)]). The DLTS spectrum is a result of thermal emission of completely charged QDs, where the thermal activa-

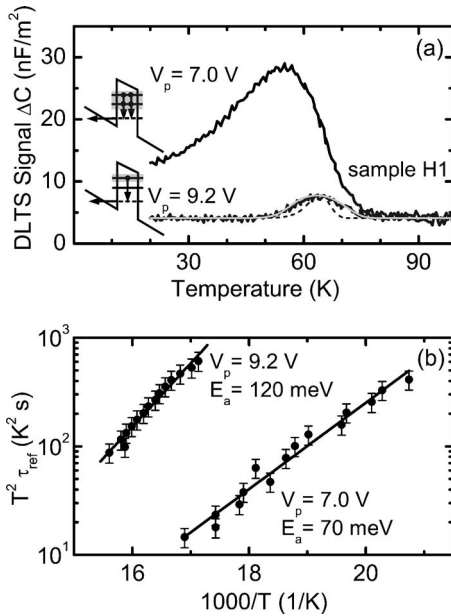


FIG. 2. DLTS spectra of thermally activated hole emission at a reference time constant of $\tau_{\text{ref}}=20$ ms, a fixed reverse bias of $V_r=9.4$ V, and a pulse length of $t_{\text{pulse}}=10$ ms (a). For a pulse bias of $V_p=7.0$ V, the QDs are completely filled with holes [schematically depicted on the left-hand side in (a)], while for $V_p=9.2$ V only the hole ground states are occupied. The black dashed line represents a simulated DLTS spectrum, that stems from thermal emission from a single energy level. The solid gray line displays a simulation, assuming an energy broadened ensemble of QDs with a Gaussian shape and a FWHM of 30 meV. Panel (b) displays the Arrhenius plots for both filling pulses, yielding activation energies of 70 meV ($V_p=7.0$ V) and 120 meV ($V_p=9.2$ V), respectively.

tion energy of each emitted hole depends on the actual charge state. As a consequence, the DLTS peak is broadened and extends toward temperatures below 20 K.

The thermal emission rate e_{thermal} is usually given by^{17,30}

$$e_{\text{thermal}} = \gamma T^2 \sigma_{\infty} \exp(-E_a/kT), \quad (1)$$

where E_a is the activation energy, σ_{∞} is the capture cross section for $T=\infty$, and γ is a temperature-independent constant. From an Arrhenius plot [$V_p=7.0$ V in Fig. 2(b)] of the DLTS peak position for varying reference time constants τ_{ref} we obtain an average apparent activation energy of about (70 ± 10) meV.

In order to study the charge carrier activation energies with more precision, we can use the charge-selective DLTS method.²² This technique always sets the pulse bias in relation to the reverse bias, such that on average the thermal emission of about one charge carrier per QD is probed. By changing the reverse bias, this method allows one to control the QDs charge state (see Geller *et al.*).²² For a pulse bias of $V_p=9.2$ V, we filled only the ground states with approximately one hole per QD. As a consequence, a narrower peak at about $T=60$ K appears in Fig. 2(a), while no DLTS signal below 50 K exists. From an Arrhenius plot [$V_p=9.2$ V in Fig. 2(a)], we obtain an apparent activation energy of

(120 ± 10) meV with a capture cross section of about $\sigma_{\infty}^{H1} \approx 7 \times 10^{-14}$ cm².

Even the DLTS curve for $V_p=9.2$ V does not represent a single emission process, as we always probe an energy broadened ensemble of QDs. For comparison, the black dashed line in Fig. 2(a) displays a simulated DLTS spectrum [using Eq. (1)], that stems from thermal emission from a single energy level. This simulation clearly shows a smaller peak width than the experimental data (black solid line for $V_p=9.2$ V). The solid gray line in Fig. 2(a) displays a simulation that was fitted to the experimental data, assuming thermal emission from an energy broadened ensemble of QDs. We obtained good agreement with the experimental data for a Gaussian shape with a full width of half maximum (FWHM) of 30 meV.

As expected, the activation energy of 120 meV from the charge-selective DLTS is much larger than the value of 70 meV from multiple hole emission, where a number of more weaker bound states are involved. However, it is evident that this value still underestimates the ground-state localization energy, if we compare it with the theoretical prediction from eight-band $\mathbf{k} \cdot \mathbf{p}$ theory.¹⁵ For QDs with a base length of ~ 16 nm, a hole ground-state localization of about 200 meV is predicted. Previous admittance spectroscopy measurements from Chang *et al.*²⁵ confirm our DLTS measurements and explain also the significant underestimation of the hole localization energy caused by a two-step emission process: The thermal activation into an excited state and subsequent tunneling through the tip of the remaining triangular barrier [bottom schematic picture in Fig. 2(a)].

For the electrons in sample E1, the apparent thermal activation energies are even smaller. In the charge-selective DLTS measurements of sample E1, for a reverse/pulse bias of 6.8 V/6.0 V only an energy broadened ensemble of electron ground states are charged with approximately one electron per QD [cf. the C - V measurement of sample E1 in Fig. 1]. A single DLTS peak occurs at about 50 K for a reference time constant $\tau_{\text{ref}}=30$ ms. The corresponding apparent thermal activation energy is (82 ± 10) meV (not shown here), representing—as previously demonstrated²⁰—the ground to first excited state level splitting. As electrons have a larger tunneling probability than holes for the same barrier height, thermal activation excites electrons mainly to the first excited state before tunneling through the remaining triangular barrier takes place. The apparent thermal activation energy is, thus, more reduced for electrons than for holes. In addition, we obtain from an Arrhenius plot a capture cross section of about $\sigma_{\infty}^{E1} \approx 2 \times 10^{-14}$ cm².

C. Time-resolved tunneling capacitance measurements

We first recorded capacitance transients for increasing temperature to ensure for the subsequent TRTCM investigations, that the observed change in the capacitance is only due to tunneling. In general, the capacitance reflects the population of the QDs with majority charge carriers. In Fig. 3, for instance, the minimum capacitance at $t=0$ represents the maximum population of the QD ground states with holes. For $t>0$ an increasing capacitance is caused by a decreasing

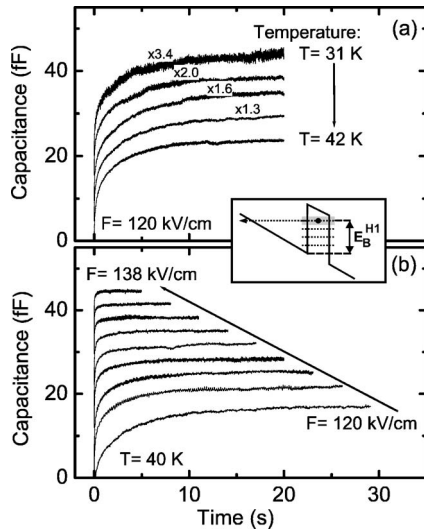


FIG. 3. Capacitance transients for increasing temperature from 31 K up to 42 K at a reverse bias of $V_r=10.4$ V (a). The reverse bias corresponds to an electric field of 120 kV/cm in the QD layer of sample H1. The almost constant emission time proves that no thermal emission is present and pure hole tunneling is observed. When increasing the applied electric field from 120 kV/cm up to 138 kV/cm, the emission time decreases significantly in (b). The pulse bias $V_p=9.2$ V was set such that, on average, only the hole ground states are occupied and tunneling through the entire barrier E_B^{H1} is observed (see schematic inset). The pulse width was set to $t_{\text{pulse}}=900$ ms and the transients are vertically shifted for clarity.

hole population due to tunneling emission. The filling pulse is not shown in the following TRTCM spectra, i.e., the capacitance transients begin at the time when the tunneling emission process starts.

Figure 3(a) displays capacitance transients at temperatures between 31 K and 42 K. The reverse bias was set to $V_r=10.4$ V, which corresponds to an electric field of about 120 kV/cm in the QD layer. The electric field was determined based on a simple approximation for p - n junctions,³¹ see the Appendix. The pulse bias was adjusted to $V_p=9.2$ V, such that on average only the hole ground states are filled. An almost constant emission time with an average value of (2.1 ± 0.3) s is obtained, which proves that pure hole tunneling is observed in this temperature range. In the charge-selective DLTS measurement in Fig. 2, the peak starts at about $T=45$ K for identical reverse/pulse bias situation, due to the initiation of the thermal hole emission on a 20 ms time scale. Thermally activated emission also occurs in the TRTCM spectra [Fig. 3(a)] for $T>45$ K, leading to a decreasing emission time with increasing temperature (not shown). Note the minor effect of an increasing amplitude of the transients with increasing temperature [Fig. 3(a)]. The QD charging process is slightly temperature dependent, due to the fact that the charge carriers have to overcome an electrical potential barrier from the reservoir into the QDs if the pulse bias is not set to flat-band condition.

A strong dependence of the tunneling emission time on the applied electric field is visible in Fig. 3(b), which is an additional confirmation of pure hole tunneling. From the recorded capacitance transients, we are now able to obtain hole

tunneling times from the QD ground states through the GaAs barrier E_B^{H1} (sample H1 on the right-hand side in Fig. 6). As mentioned before, we observe carrier emission from an energy broadened ensemble of QDs, hence, the capacitance transients cannot be described by a single exponential. Different single QDs with varying size, shape, and composition are expected to have different tunneling rates. As a consequence, we observe tunneling emission with different time constants, leading to multiexponential transients.

Figure 5(a) depicts three selected capacitance transients from Fig. 3(b) as gray lines on a semilogarithmic scale. Clearly visible is a nonexponential decay, as in DLTS experiments on deep levels in semiconductor alloys (see Omling *et al.*,³² and references therein). The capacitance transients $C(t)$ are fitted with a so-called stretched exponential function (see Scher *et al.*,³³ and references therein):

$$C(t) = C(t_0) \exp[-(t/\tau^*)^\beta]. \quad (2)$$

Equation (2) describes a superposition of different exponential tunneling processes, with τ^* being an effective time constant and β as the stretching parameter. The latter describes the spread of time constants and is unity for a monoexponential decay. A stretching parameter below one indicates a variation from a monoexponential transient. By probing an ensemble of QDs with a FWHM of about 30 meV (see before), the capacitance transients of the tunneling emission can be fitted well by Eq. (2) (black lines in Fig. 5), with a stretching parameter of about 0.6. The tunneling times of sample H1, as function of the applied electric field, are shown as gray dots on the right-hand side in Fig. 6. In addition, we evaluated the $1/e$ -decay time as an average emission time of the ensemble (black dots in Fig. 6). The tunneling times have an accuracy of about 20%. The tunneling time decreases for sample H1 from about 2 s down to 30 ms for an increasing electric field from 120 kV/cm (at $V_r=10.4$ V) to 138 kV/cm (at $V_r=12.5$ V). The solid lines are fits to the data, as predicted from Eq. (3) (see below).

The electron tunneling emission from the ground states through the GaAs barrier E_B^{E1} is shown in Fig. 4 on a linear scale. Here, the pulse bias was set to $V_p=6.0$ V. Hence, only the ground states are occupied with electrons (see schematic inset in Fig. 4). At $T=20$ K, the thermal electron emission can be neglected. The decrease in the population of the QD ground states was recorded time resolved. Figure 5(b) depicts three selected capacitance transients from Fig. 4 as gray lines on a semilogarithmic scale. Once again, a nonexponential decay is clearly visible, which we fitted with a stretched exponential function [black lines in Fig. 5(b)]. The effective time constants τ^* are shown as gray dots on the left-hand side in Fig. 6 (sample E1). The $1/e$ -decay times are displayed as black dots. Increasing the electric field from 79 kV/cm (at $V_r=7.0$ V) up to 92 kV/cm (at $V_r=8.0$ V) reduces the tunneling time from about 5 s down to 80 ms.

IV. ANALYSIS AND DISCUSSION

The GaAs barrier height for electrons E_B^{E1} and holes E_B^{H1} can be obtained from the dependence of the tunneling time on the applied electric field. The barrier height is almost

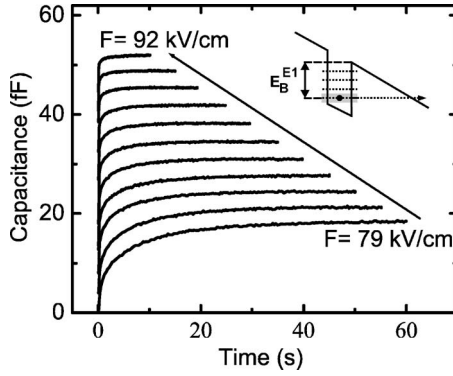


FIG. 4. Electron tunneling from the ground states through the GaAs barrier E_B^{E1} for sample E1, observed in capacitance transients at low temperature ($T=20$ K). The pulse bias V_p was set to 5.8 V to occupy only the electron ground states (see inset), while the reverse bias was increased to apply an electric field from 79 kV/cm up to 92 kV/cm. The pulse width was set to $t_{\text{pulse}}=900$ ms and the transients are vertically shifted for clarity.

equal to the entire localization energy E_{loc} . The difference is due to the Poole-Frenkel effect,³⁴ which slightly lowers the barrier height in an applied electric field: $\Delta E_{\text{PF}}=eFh/2$, where F is the electric field and h is the QD height. The localization energy E_{loc} is the sum of the tunneling barrier height and an estimated Poole-Frenkel energy ΔE_{PF} (see schematic inset in Fig. 7). The Poole-Frenkel effect reduces—for QDs (Ref. 35) with an average height of 4 nm—the hole barrier by approximately 24 meV for an electric field of ~ 120 kV/cm. For electrons, the barrier height is reduced by approximately 16 meV for an electric field of about 80 kV/cm. The accuracy of ΔE_{PF} is limited by the knowledge of the QD height. The Poole-Frenkel effect,

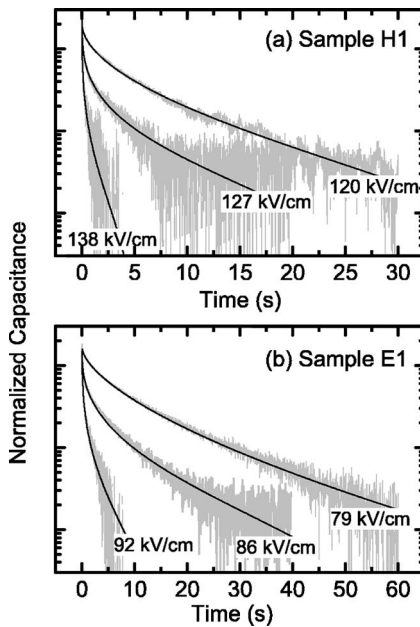


FIG. 5. Capacitance transients of hole (a) and electron tunneling (b), displayed on a semilogarithmic scale. Only three transients from Figs. 3(b) and 4 are shown for clarity. Black solid lines are fits with stretched exponential functions.

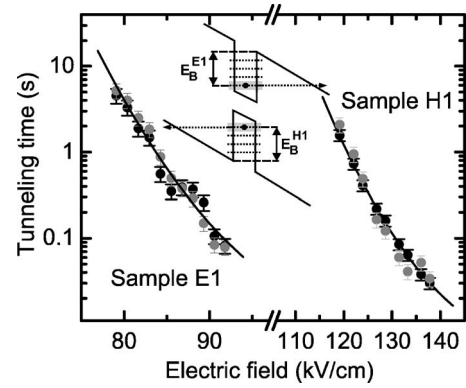


FIG. 6. Electron (sample E1) and hole (sample H1) tunneling times. The tunneling times were obtained by evaluation of the $1/e$ decay time (black dots) and stretched exponential fits (gray dots). The solid lines are fits to the data. The inset displays schematically the tunneling process through the GaAs barrier E_B for electrons and holes.

however, has only a minor impact on the determination of the localization energy.

The tunneling rate is needed to obtain the barrier height E_B from the experimental data. Fry *et al.*³⁶ modeled the tunneling rate e_{tunnel} using an adiabatic approximation, where the tunneling probability depends only on the z part (parallel to the electric field) of the wave function. Using an one-dimensional (1D) Wentzel-Kramer-Brillouin calculation,³⁷ for an 1D potential with height h , the tunneling rate e_{tunnel} is given by

$$e_{\text{tunnel}} = \frac{\hbar \pi}{2m^* h^2} \exp \left[\frac{-4}{3 \hbar F e} \sqrt{2m^* E_B^3} \right], \quad (3)$$

where m^* is the GaAs effective mass. The exponential factor is the common expression for the transparency of a triangular barrier. In the following, only the exponential factor is rel-

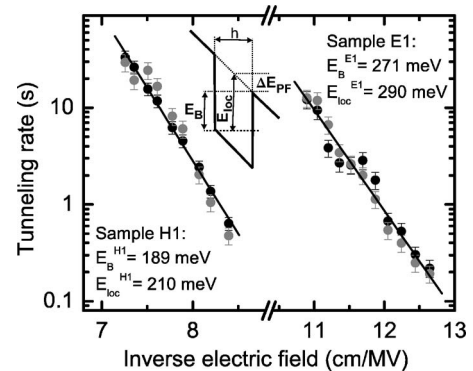


FIG. 7. Tunneling rate for holes (sample H1) and electrons (E1) as function of the inverse electric field. From the linear dependence, as predicted in Eq. (3), we obtain a hole ($E_B^{H1}=189$ meV) and electron barrier height ($E_B^{E1}=271$ meV). Adding an approximate value for the Poole-Frenkel energy ΔE_{PF} leads to the hole $E_{\text{loc}}^{H1}=210$ meV and electron $E_{\text{loc}}^{E1}=290$ meV localization energy (schematic inset).

evant to obtain the tunneling barrier height, and the prefactor will be neglected.

As predicted by Eq. (3), a linear dependence of the tunneling rate on a logarithmic scale via the inverse electric field occurs in Fig. 7. A hole barrier height of ($E_B^{\text{H1}} = 189 \pm 11$) meV can be determined from a linear fit to the data. The accuracy is mainly limited by the uncertainty of the heavy hole effective mass. For the [100] direction—which is the growth and tunneling direction—the GaAs heavy hole effective mass is $m^* = 0.40 m_0$,³⁸ with a standard deviation of $0.06 m_0$. A minor limitation of the accuracy is given by the determination of the electric-field strength (see the Appendix). From a linear fit of the electron sample data (Fig. 7), we are also able to determine an electron barrier height of $E_B^{\text{E1}} = (271 \pm 24)$ meV. Here, we used the recommended value for the GaAs electron effective mass^{39,40} of $0.0635 m_0$.⁴¹

The hole and electron ground-state localization energy is the sum of the barrier height E_B and the estimated energy lowering due to the Poole-Frenkel effect ΔE_{PF} (see the schematic inset in Fig. 7): $E_{\text{loc}} = E_B + \Delta E_{\text{PF}}$. The hole and electron localization energies are: $E_{\text{loc}}^{\text{H1}} = (210 \pm 20)$ meV and $E_{\text{loc}}^{\text{E1}} = (290 \pm 30)$ meV, respectively.⁴² The eight-band $\mathbf{k} \cdot \mathbf{p}$ theory¹⁵ predicts a hole ground-state localization energy of ~ 200 meV for QDs with a base length of about 16 nm (as in sample H1). The electron localization energy is in the order of 280 meV (for QDs with a base length of about 18 nm). Therefore, the electron/hole ground-state localization energies obtained experimentally from the TRTCM method are in excellent agreement with the theoretical predictions.

To verify the localization energies, we estimated the theoretical values of the tunneling times using Eq. (3). The theoretical hole tunneling time for a localization energy of 210 meV and an approximate QD height of 4 nm (from TEM images, Sec. II) decreases from about 2.3 s ($F = 120$ kV/cm) down to 30 ms ($F = 138$ kV/cm). Assuming the same QD height and using the energy of 290 meV leads to a decreasing electron tunneling time from 2.2 s ($F = 79$ kV/cm) down to 20 ms ($F = 92$ kV/cm). The theoretical tunneling times are in good agreement with the values from the experiments.

The escape time for *thermal excitation* from the electron/hole ground states can be estimated by using Eq. (1), the capture cross sections in Sec. III B, and the localization energies for sample E1/H1, respectively. For zero-electric field, an average thermal escape time at room temperature for electrons of about 200 ns and for holes of about 0.5 ns is obtained.

V. CONCLUSION

We have reported the observation of tunneling escape from self-organized In(Ga)As/GaAs QDs in time-resolved capacitance measurements. The observed escape time is temperature-independent, but depends strongly on the applied electric field in the QD layer. The electron tunneling time decreases from about 5 s at 79 kV/cm down to 80 ms at 92 kV/cm, while the hole tunneling time decreases from about 2 s at 120 kV/cm down to 30 ms at 138 kV/cm.

TRTCM allows us to determine the electron and hole ground-state localization energy by measuring the dependence of the tunneling time constant as function of the electric field. The experimental values of $E_{\text{loc}}^{\text{H1}} = (210 \pm 20)$ meV for the hole and $E_{\text{loc}}^{\text{E1}} = (290 \pm 30)$ meV for the electron localization are in excellent agreement with predictions from the eight-band $\mathbf{k} \cdot \mathbf{p}$ theory. Based on these values, we estimated the thermally activated escape time at room temperature as ~ 200 ns for electrons and ~ 0.5 ns for holes in case of a zero-electric field situation.

ACKNOWLEDGMENTS

This work was funded by the SANDiE Network of Excellence of the European Commission, contract No. NMP4-CT-2004-500101, and SFB 296 of DFG. We would like to thank A. Marent for providing the DLTS simulation program.

APPENDIX: DETERMINATION OF THE ELECTRIC FIELD

We determined the electric field at the position of the QD layer x using the common equation for an electric field F across the depletion region of an abrupt p-n junction³¹

$$F(x) = \frac{eN_a}{\epsilon}(w - x). \quad (\text{A1})$$

The expression for the width of the depletion region w can be written as

$$w = \sqrt{\frac{2\epsilon N_a + N_b}{e N_a \cdot N_b} (V_{\text{bi}} + V_r)}, \quad (\text{A2})$$

where ϵ is the dielectric constant in GaAs and V_{bi} the built-in potential. N_a is the doping concentration in the matrix material, surrounding the QD layer. N_b is the doping concentration of the highly doped top layer, i.e., the n^+ or p^+ contact of sample H1/sample E1, respectively.

Equations (A1) and (A2) describe an idealized model in which the boundary at the edge of the depletion region is abrupt, and beyond the depletion region the GaAs is electrically neutral. It is a good practical approximation to obtain the width of the depletion region and the strength of the electric field.³⁰ This simple approximation characterizes a p - n junction without an embedded QD layer, which pins the depletion region, as is clearly visible in the static C - V measurements in Fig. 1. Nevertheless, during the tunneling emission of the charge carriers, the QDs are completely inside the space-charge region for all applied reverse biases and only charged with up to one charge carrier per QD. Therefore, we can assume that Eq. (A1) is reasonable to determine the electric field, since we assume that almost uncharged QDs have only a minor effect on the width of the depletion region and, hence, on the strength of the electric field.

The assumption can be easily confirmed by a simple estimate of the influence of singly charged QDs on the depletion region: For a QD sheet density of about $N_D^{\text{QD}} \approx 3 \times 10^{10}$ cm⁻² and a depletion width always larger than 700 nm for all applied reverse biases, the QD charge is equivalent to a

space-charge concentration less than $N_D^{SC} \approx 4 \times 10^{14} \text{ cm}^{-3}$. This value is almost two orders of magnitude smaller than the doping concentration, which determines—in addition to the applied reverse bias V_r —the width of the depletion region and the magnitude of the electric field. The error in the determination of the electric field due to the assumption of singly charged QDs is estimated to always be smaller than 0.5 kV/cm. Therefore, the influence of the charged QDs can be neglected.

The accuracy of the determination of the applied electric

field is, hence, mainly due to the uncertainty of the doping concentration N_a . We determine the doping concentration from static C - V measurements to $N_a^{H1} = (1.6 \pm 0.3) \times 10^{16} \text{ cm}^{-3}$ and $N_a^{E1} = (2.0 \pm 0.3) \times 10^{16} \text{ cm}^{-3}$ at the tunneling measurement temperature of $T = 40 \text{ K}/20 \text{ K}$ for sample H1/E1, respectively. This differs from the nominal doping concentration. Note, that even with an uncertainty of about 20% for the doping concentration, N_a , the total accuracy of the electric field is better than 5% due to the error propagation theorem.

*Electronic address: geller@physik.tu-berlin.de

†Present address: Robert Bosch GmbH, Tübinger Strasse 123, 72762 Reutlingen, Germany.

¹D. Bimberg, M. Grundmann, and N. N. Ledentsov, *Quantum Dot Heterostructures* (Wiley, Chichester, 1998).

²Y. Arakawa and H. Sakaki, *Appl. Phys. Lett.* **40**, 939 (1982).

³N. Kirstaedter, N. N. Ledentsov, M. Grundmann, D. Bimberg, V. M. Ustinov, S. S. Ruvimov, M. V. Maximov, P. S. Kop'ev, Z. I. Alferov, U. Richter *et al.*, *Electron. Lett.* **30**, 1416 (1994).

⁴F. Heinrichsdorff, C. Ribbat, M. Grundmann, and D. Bimberg, *Appl. Phys. Lett.* **76**, 556 (2000).

⁵M. Kuntz, G. Fiol, M. Lämmlin, D. Bimberg, M. G. Thompson, K. T. Tan, C. Marinelli, R. V. Penty, I. H. White, V. M. Ustinov *et al.*, *Appl. Phys. Lett.* **85**, 843 (2004).

⁶P. Michler, A. Kiraz, C. Becher, W. V. Schoenfeld, P. M. Petroff, L. Zhang, E. Hu, and A. Imamoglu, *Science* **290**, 2282 (2000).

⁷C. Santori, D. Fattal, J. Vučković, G. S. Solomon, and Y. Yamamoto, *Nature (London)* **419**, 594 (2002).

⁸J. C. Campbell, D. L. Huffaker, H. Deng, and D. G. Deppe, *Electron. Lett.* **33**, 1337 (1997).

⁹L. Chu, A. Zrenner, M. Bichler, and G. Abstreiter, *Appl. Phys. Lett.* **79**, 2249 (2001).

¹⁰S. Muto, *Jpn. J. Appl. Phys., Part 1* **34**, 210 (1995).

¹¹S. M. Sze, in *Future Trends in Microelectronics*, edited by S. Luryi, J. Xu, and A. Zaslavsky (Wiley, New York, 1999), p. 291.

¹²T. Lundstrom, W. Schoenfeld, H. Lee, and P. M. Petroff, *Science* **286**, 2312 (1999).

¹³H. Pettersson, L. Baath, N. Carlson, W. Seifert, and L. Samuelson, *Appl. Phys. Lett.* **79**, 78 (2001).

¹⁴M. Kroutvar, Y. Ducommun, D. Heiss, M. Bichler, D. Schuh, G. Abstreiter, and J. J. Finley, *Nature (London)* **432**, 81 (2004).

¹⁵O. Stier, M. Grundmann, and D. Bimberg, *Phys. Rev. B* **59**, 5688 (1999).

¹⁶C. T. Sah, L. Forbes, L. L. Rosier, and A. F. Tasch, Jr., *Solid-State Electron.* **13**, 759 (1970).

¹⁷D. V. Lang, *J. Appl. Phys.* **45**, 3023 (1974).

¹⁸S. Anand, N. Carlsson, M.-E. Pistol, L. Samuelson, and W. Seifert, *Appl. Phys. Lett.* **67**, 3016 (1995).

¹⁹C. M. A. Kapteyn, F. Heinrichsdorff, O. Stier, R. Heitz, M. Grundmann, N. D. Zakharov, D. Bimberg, and P. Werner, *Phys. Rev. B* **60**, 14265 (1999).

²⁰C. M. A. Kapteyn, M. Lion, R. Heitz, D. Bimberg, P. N. Brunkov, B. V. Volovik, S. G. Konnikov, A. R. Kovsh, and V. M. Ustinov, *Appl. Phys. Lett.* **76**, 1573 (2000).

²¹C. M. A. Kapteyn, M. Lion, R. Heitz, D. Bimberg, C. Miesner, T. Asperger, and G. Abstreiter, *Appl. Phys. Lett.* **77**, 4169 (2000).

²²M. Geller, C. Kapteyn, L. Müller-Kirsch, R. Heitz, and D. Bimberg, *Appl. Phys. Lett.* **82**, 2706 (2003).

²³O. Engström, M. Malmkvist, Y. Fu, H. O. Olafsson, and E. O. Sveinbjörnsson, *Appl. Phys. Lett.* **83**, 3578 (2003).

²⁴S. Schulz, S. Schnüll, C. Heyn, and W. Hansen, *Phys. Rev. B* **69**, 195317 (2004).

²⁵W. H. Chang, W. Y. Chen, T. M. Hsu, N. T. Yeh, and J. I. Chyi, *Phys. Rev. B* **66**, 195337 (2002).

²⁶F. Guffarth, R. Heitz, A. Schliwa, O. Stier, M. Geller, C. M. A. Kapteyn, R. Sellin, and D. Bimberg, *Phys. Rev. B* **67**, 235304 (2003).

²⁷I. Mukhametzhano, R. Heitz, J. Zeng, P. Chen, and A. Madhukar, *Appl. Phys. Lett.* **73**, 1841 (1998).

²⁸F. Heinrichsdorff, *MOCVD Growth and Laser Applications of In(Ga)As/GaAs Quantum Dots* (Mensch & Buch, Berlin, 1998) [Dissertation, Technische Universität Berlin].

²⁹R. Heitz, I. Mukhametzhano, P. Chen, and A. Madhukar, *Phys. Rev. B* **58**, R10151 (1998).

³⁰P. Blood and J. W. Orton, *The Electrical Characterization of Semiconductors: Majority Carriers and Electron States* (Academic Press, London, 1992).

³¹S. M. Sze, *Semiconductor Devices—Physics and Technology* (Wiley, New York, 1985).

³²P. Omling, L. Samuelson, and H. G. Grimmeis, *J. Appl. Phys.* **54**, 5117 (1983).

³³H. Scher, M. F. Shlesinger, and J. T. Bandler, *Phys. Today* **26**, 26 (1991).

³⁴J. Frenkel, *Phys. Rev.* **54**, 647 (1938).

³⁵S. Anand, N. Carlsson, M.-E. Pistol, L. Samuelson, and W. Seifert, *J. Appl. Phys.* **84**, 3747 (1998).

³⁶P. W. Fry, J. J. Finley, L. R. Wilson, A. Lemaître, D. J. Mowbray, and M. S. Skolnick, *Appl. Phys. Lett.* **77**, 4344 (2000).

³⁷D. M.-T. Kuo and Y.-C. Chang, *Phys. Rev. B* **61**, 11051 (2000).

³⁸*Gallium Arsenide (GaAs), Valence Bands, Effective Masses*, Landolt-Börnstein, Group III Condensed Matter, Vol. 41/A1A (Springer, Berlin, 2001).

³⁹I. Vurgaftman, J. R. Meyer, and L. R. Ram-Mohan, *J. Appl. Phys.* **89**, 5815 (2001).

⁴⁰*Gallium Arsenide (GaAs), Conduction Band, Effective Masses and Related Parameters*, Landolt-Börnstein, Group III Condensed Matter, Vol. 41/A1A (Springer, Berlin, 2001).

⁴¹The effective mass of the GaAs barrier is slightly reduced, due to the seed layer below the QDs in sample E1. A simple estimation

of the fraction of InAs in the GaAs barrier leads to a reduction of the effective mass to approximately $m_e^* \approx 0.058$, an uncertainty of about 9%. However, the total accuracy of the tunneling barrier height—including the linearization uncertainty—is only

5%, due to the error propagation theorem.

⁴²If we assume a very poor accuracy of the Poole-Frenkel energy of about 50%, due to the limited knowledge of the QD height, the total accuracy of the localization energy is better than 8%.